Effect of non-muffin-tin terms on the electronic structure of transition metals: Niobium*†

N. Elyashar‡
University of Illinois, Circle Campus, Chicago, Illinois 60680
and Argonne National Laboratory, Argonne, Illinois 60439

D. D. Koelling
Argonne National Laboratory, Argonne, Illinois 60439

(Received 15 May 1975)

The effect of removing the muffin-tin approximation in a relativistic-augmented-plane-wave calculation of the electronic structure of Nb is described. The most significant effect found is that two experimentally observed orbits occur in a fully non-muffin-tin relativistic calculation which are not present in the muffin-tin calculation. The procedure for constructing the potential in the required form and the modifications to the secular equation are explicitly described.

I. INTRODUCTION

In addition to the approximations made in reducing the many-body Hamiltonian for the electronic states in solids to a one-electron problem there remains the question of a self-consistent determination of the potential to be used in the single-electron-band Hamiltonian. In the most popular methods used for transition metals such as the augmented-plane-wave (APW)[1] and Korringa-Kohn-Rostoker (KKR)[2] methods, the muffin-tin (MT) shape approximation to the potential is often used, in which the potential is replaced by a spherically symmetric potential inside a sphere inscribed in the unit cell (muffin-tin sphere) and by a constant in the interstitial region. Although this approximation to the crystal potential has given a reasonably accurate picture of the band structure and Fermi surface of transition and noble metals[3] as well as some compounds,[4] the effects of non-muffin-tin terms (NMT) on the eigenvalues, wave functions, and Fermi surface have not been fully investigated. The NMT terms are naturally decomposed into two parts[5]: (a) a contribution V_{NS} to the inside region of touching MT spheres and (b) a contribution V_{WMT} to the interstitial region. In the past few years there have been several band-structure results incorporating the effects of V_{WMT} in the calculation[6] while neglecting V_{NS}. This model is generally referred to as the warped muffin-tin (WMT) approximation.[7] In the case of transition metals, where the Fermi energy lies in a partially filled d band, the energy shifts arising from nonspherical terms inside the MT spheres may be quite significant.[8] This is primarily owing to the fact that the d states being fairly well localized (usually 80 to 90% of d charge density is inside the MT sphere) are as much affected by the potential shifts in the inside region as the outside potential shifts. Several calculations have been performed using a general (no shape approximation) potential form in the nonrelativistic approximation.[6,9-11] Of these, only Kleinman and Shurtleff deal with a transition metal (Fe). They truncated the expansion inside the MT spheres at $L=4$ and only considered its effect up to $L=2$ in the basis function so that in the nonrelativistic approximation they could include this term by merely solving the radial equation with different potentials for the t_{2g} and ϵ_g d states. Wakoh and Yamashita[12] effectively did the same thing for V and Cr by shifting the phase shifts for the two different d states. This was necessary to get a reasonable agreement with experiment. In their parametrization of the Mo and W Fermi surfaces, Ketterson *et al.*[13] also found that it was necessary to include the nonspherical corrections to the muffin-tin potential in order to obtain fits which were inside the experimental error.

Recently Painter, Faulkner, and Stocks[8] (hereafter referred to as PFS) have calculated and discussed the shifts in the eigenvalues which result from NMT terms in Rb, Nb, and Pd at high-symmetry points and along symmetry directions using the Korringa-Kohn-Rostoker discrete variational method[14] (KKR-DVM) in the nonrelativistic approximation. Their results indicate energy shifts of the order of 2–10 mRy, the shifts being largest for Nb and nearly zero for Rb.

In this paper, we will describe the techniques we have used to include NMT effects in relativistic augmented-plane-wave (RAPW) calculations and consider their effects on a simple model. Primarily as an illustrative example, we present here the results of including the NMT terms on the band structure of Nb calculated in the overlapping charge-density model using the Slater-exchange approximation. This is a particularly useful ex-

ample in that the same model-potential construction was used by Mattheiss[15] to obtain the nonrelativistic MT bands (which compare reasonably well with the de Haas–van Alphen data[16]) and by PFS in their investigation of NMT effects. We find: (a) A full treatment of this model predicts two orbits seen experimentally but not present in the MT calculations. Other orbits are also tentatively predicted which will be looked for in future experiments. (b) Although in agreement with PFS on the size of the effects of the nonspherical terms inside the muffin-tin spheres, we find the potential correction in the interstitial region (WMT) to be larger than they do. This is discussed in terms of the basis functions used.

As this is a test to assess the significance of these terms and the techniques for dealing with them before proceeding to a full self-consistent-field (SCF) calculation, comparison to experiment and the results of others will be brief. We here focus on the sensitivity to the NMT terms, the techniques used, and the convergence properties of various expressions which must be truncated. We will report a full comparison using the fully SCF results when those calculations are completed.

II. METHOD

A. Construction of non-muffin-tin potential

Since the APW basis functions have a dual representation, i.e., plane waves in the interstitial region and a spherical harmonic expansion inside the MT spheres, it is appropriate to consider the same dual representation for the density and potential. Thus:

$$V(\vec{r}) = \begin{cases} \sum_{\nu} V_{\nu}(r)\, K_{\nu}(\hat{r}) & r \leq R, \\ \sum_{n} V(\vec{K}_n) e^{i \vec{K}_n \cdot \vec{r}} & r \geq R. \end{cases} \tag{1}$$

We will refer to this as the general potential (GP) as it contains no shape approximations beyond the truncation of the series. To construct the potential, the spherically symmetric atomic density of Nb with configuration $4d^4 5s$ was superimposed to generate an approximate crystal charge density. The lattice constant for Nb is chosen to be 6.237 74 a.u. which is the same as the value used by Anderson *et al.*[17] in their SCF calculation for Nb. The MT sphere radius is taken to be approximately 2.64 a.u. for the nonoverlapping MT spheres. The charge inside the MT spheres was decomposed into angular momentum components, whereas the charge in the interstitial region was Fourier analyzed. Owing to cubic symmetry only certain linear combination of spherical harmonics,[18] i.e., the well-known cubic harmonics, will survive. To check the convergence of the two series, the charge density from the interstitial region Fourier expansion was calculated at the MT sphere boundary and compared to the values obtained from the cubic harmonic expansion of the interior.

The construction of this dual representation of the charge density for the overlapping charge-density model is straightforward.[19] We thus start with the dual representation for the charge density

$$\rho(\vec{r}) = \begin{cases} \sum_{l} \rho_l(r) K_l(\hat{r}) - 2Z\delta_0(r) & \text{for } r \leq R, \\ \sum_{n} \rho^n e^{i \vec{K}_n \cdot \vec{r}} & \text{for } r \geq R, \end{cases} \tag{2}$$

which is the form that would naturally be obtained from the RAPW wave functions in an SCF calculation. Here R is the radius of an MT sphere, Z is the atomic number, $\vec{K}_n$ is a vector of reciprocal-lattice space, and $K_l(\hat{r})$ are the cubic harmonics. In Eq. (2) we have used atomic units and we have multiplied the charge density by $-e$, the charge of an electron.

The Coulomb potential is constructed first. In order to avoid the complicated real space part of the Ewald sums which arise in superimposing the multipole potentials, we reorganize Eq. (2) such that the potential consists of three parts arising from: (a) a neutral spherical charge-density "pseudoatom" within the muffin-tin spheres about each atomic site, (b) the multipole moments within the MT spheres, and (c) the background charge extending throughout the zone. The neutral pseudoatom potential is easily obtained by straightforward integration and the background potential by Fourier analysis. The displaced multipole potentials can be expanded around the central cell using the well-known properties of the spherical harmonics.[19]

To construct the potential we rewrite this representation of $\rho(\vec{r})$ by continuing the plane-wave part smoothly inside the MT sphere and subtracting it out we can write

$$\rho(\vec{r}) = \left(\sum_{l} \rho_l(r) K_l(\hat{r}) - \sum_{n} \rho^n e^{i \vec{K}_n \cdot \vec{r}} \right) \theta_0(r) + \sum_{n} \rho^n e^{i \vec{K}_n \cdot \vec{r}} - 2Z\delta_0(r), \tag{3}$$

where $\theta_0(r)$ is a step function which has the value one inside the muffin-tin sphere and zero outside for each cell.

To do the Ewald decomposition, we add and subtract a density $(\epsilon^3/\pi^{3/2})\rho^0 \Omega e^{-\epsilon^2 r^2}$ choosing the Ewald parameter ϵ such that the Gaussian can be approximated as entirely inside the muffin-tin sphere. (The value 2.3 was actually used.) ρ^0 is

the $\vec{K}=0$ Fourier component of the charge density and Ω is the volume of unit cell. Then one can write

$$\rho(\vec{r})=\rho_a(\vec{r})+\rho_{NFE}(\vec{r}), \tag{4}$$

where

$$\rho_a(\vec{r})=\Big(\sum_l \rho_l(r)K_l(\hat{r})-\sum_n \rho^n e^{i\vec{K}_n\cdot\vec{r}} + \frac{\epsilon^3}{\pi^{3/2}}\rho^0\Omega e^{-\epsilon^2 r^2}-2Z\delta_0(r)\Big)\theta_0(r), \tag{5}$$

$$\rho_{NFE}(\vec{r})=\sum_{n\neq 0}\rho^n e^{i\vec{K}_n\cdot\vec{r}}+\rho^0-\frac{\epsilon^3}{\pi^{3/2}}\rho^0\Omega e^{-\epsilon^2 r^2}.$$

As is seen from the above construction the integral of ρ_a over the MT sphere vanishes. Expanding the plane-wave part inside the MT spheres in cubic harmonics and adding it term by term to the sum $\sum_l \rho_l K_l$, and Fourier transforming the Gaussian we obtain a similar expansion[19] for the "pseudoatom"

$$\rho_a=\sum_l \tilde{\rho}_l(r)K_l(\hat{r})-2Z\delta_0(r) \tag{6}$$

which is for a neutral entity within the muffin-tin sphere. As such the explicit statement that r is less than the muffin-tin radius can be dropped. Fourier transforming the compensating Gaussian which must be subtracted from the plane-wave expansion (which has been extended into the muffin-tin spheres), one obtains the modified plane-wave contribution

$$\rho_{NFE}=\sum_n(\rho^n-\rho^0 e^{-K_n^2/4\epsilon^2})e^{i\vec{K}_n\cdot\vec{r}}. \tag{7}$$

The Coulomb potential is then readily obtained as a combination of the standard results for the multipole expansion and the Fourier expansion.

Within the muffin-tin spheres, the displaced multipole (other site) potentials can be expanded about the origin[20] to put the results in the form required [Eq. (1)]. This treatment of the higher multipole moments of ρ_a necessitates two truncations. First, one must truncate the lattice summation. Since ρ_a has been constructed to be neutral, there is no other site contribution from $\tilde{\rho}_0$. And the terms for $\tilde{\rho}_4$ and $\tilde{\rho}_6$ decrease as $(1/T)^{L+1}$ where T is a lattice vector, so the lattice sum can be performed directly. (In practice, we included 11 near-neighbor shells in this sum.) Second, the expansion of the displaced multipoles introduces high-order terms. However, this expansion in even L is rapidly convergent with the expansion parameter $(r/T)^2<\frac{1}{4}$. The largest term omitted is of the order of $(r/T)^{13}$ which we believe to be a quite adequate treatment of these very small terms.

The $L>4$ multipole contributions also extend into the interstitial region and this contribution must be Fourier analyzed. This can be done analytically[19] using the simple expedient of extending these terms into the muffin-tin sphere region. As this extension merely selects a unique Fourier-series expansion (which need only converge to the multipole terms in the interstitial region), we may select this extension for our convenience—in this case, rapid convergence. The functional form actually used was a radial function $(A_L r^L + B_L r^{L-1})$ multiplying the cubic harmonic. This resultant analytic form for the Fourier-series expansion of these terms converges as $(1/K_n R)^4$. In these calculations, we used 81 stars which is far in excess of what was required. Thus we have constructed the required dual representation of the Coulomb potential.

Next we add to this the exchange contribution. We have used here Slater's free-electron approximation[21]

$$V_{ex}(\vec{r})=-6\alpha[(3/8\pi)\rho(\vec{r})]^{1/3}, \tag{8}$$

where $\rho(\vec{r})$ is the local density of electrons and α is chosen to be unity. Writing

$$\rho(\vec{r})=\rho_0(r)+\rho_4(r)K_4(\hat{r})+\rho_6(r)K_6(\hat{r})+\cdots, \quad r\leq R, \tag{9}$$

for the region inside the MT sphere, we note that ρ_0 is much larger than $\rho_4+\rho_6$ and therefore we consider a Taylor expansion of Eq. (9)

$$V_{ex}(\vec{r})=-\left(\frac{3}{\pi}\right)^{1/3}\times\left(3\rho_0^{1/3}+\frac{\rho_4}{\rho_0^{2/3}}K_4(\hat{r})+\frac{\rho_6}{\rho_0^{2/3}}K_6(r)+\cdots\right). \tag{10}$$

For the region between the MT spheres we use a fitting technique.[6,7] In this method one takes a random sample of points outside the MT sphere, finds $\rho^{1/3}(\vec{r})$ at these points, and then does a least-square Fourier fit to these values. The procedure gives accurate results (better then 0.01%) for a random sample of about 200 points and 20 stars of reciprocal-lattice vectors.

This completes the construction of the potential in the required dual representation. However, it is useful to adjust the zero of energy such that the average potential in the interstitial region $\bar{V}$:

$$\bar{V}=V(\vec{K}_n=0)-\frac{4\pi R^3}{\Omega-\frac{4}{3}\pi R^3}\sum_{n\neq 0}V(\vec{K}_n)\frac{j_1(K_nR)}{K_nR} \tag{11}$$

is zero.

In Fig. 1, the radial components of the $L=4$ and

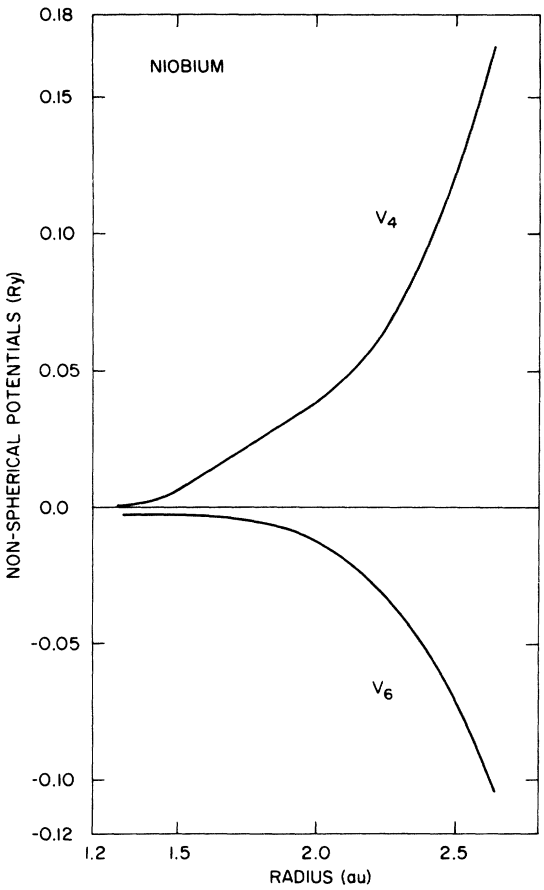

FIG. 1. Nonspherical radial components of the cubic harmonic expansion. Although these components have the opposite sign, their effect is roughly additive as can be seen from a plot of the cubic harmonics (Fig. 3).

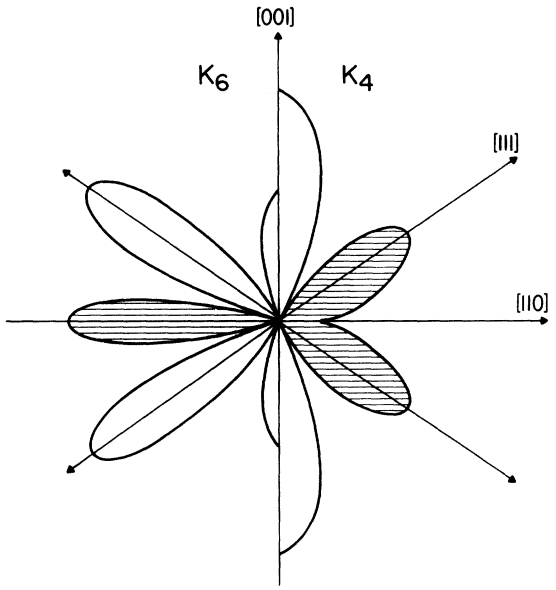

FIG. 2. Plot of the $l=4$ and $l=6$ cubic harmonics in a plane perpendicular to the $[1\bar{1}0]$ direction. Lobes marked with dashes are negative. As the bcc nearest-neighbor atom is along the [111] direction, one can see that the V_4 and V_6 terms (Fig. 2) would both add to bonding of nearest neighbors.

$L=6$ terms of the crystal potential are shown for the overlapping charge-density model of Nb. As an aid to the reader, Fig. 2 shows the angular variation of the cubic harmonics. These nonspherical terms are quite negligible in the vicinity of the nucleus where the nuclear potential and associated spherical (in this model) atomic density dominates. However, near the MT boundary, the nonspherical terms grow until they are the same size as the spherical term. This is a natural consequence of the fact that if the muffin-tin approximation were to be exact for this case, the spherical component would go to zero—to be continuous with the MT "floor" which is zero by construction. In the Nb model considered here, the MT potential has a discontinuity of 0.13 Ry. Although the radial parts of V_4 and V_6 have opposite signs, when multiplied by the corresponding angular functions, their effects on the matrix elements to be discussed below are additive rather than cancelling. (See Fig. 2.)

As one has used two very different representations in the two regions inside and outside the MT spheres, it is possible to make checks on the precision of the formulation by comparing them at the MT sphere surface where they should yield the same result. If one performs a cubic harmonic decomposition of the Fourier-series expansion and compares this to that obtained directly inside the MT spheres, one checks the precision of the exchange $\rho^{1/3}$ expansion inside the spheres and the numerical fitting in the interstitial region. Nothing is learned about the multipole lattice sum truncation as this was the same for both the inside and the outside expansions. The results agreed to within the numerical noise of the fitting (0.01%). This is reassuring as the MT boundary is the worst case for the linear expansion. In light of this good agreement for the spherical harmonic components, it is possible to get quite different information by comparing the actual values calculated as these expansions involve very different truncations. The Fourier-series expansion is truncated in reciprocal-lattice space but contains all L values. Further, from the previous test, we can expect that its convergence is excellent. Thus, by comparing the values of the two expansions, one can gauge the error resulting from truncation of the cubic harmonic expansion at $L=6$. One finds that the largest error is now 0.01 Ry which can be

immediately compared to the 0.13 Ry for the muffin-tin approximation. If the nonspherical terms result in corrections ≤ 0.007 Ry, that omitted by the truncation must have an effect which is less than 0.001 Ry (our goal) just from arguments based on size alone. But further, the next $L=8$ term will at worst couple a d-type orbital with one of $L=6$ character.

B. Matrix elements

Using the dual representation of crystal potential obtained above, one has to solve for the eigenvalues and eigenfunctions of the Dirac equation for a relativistic electron in a periodic potential[22]:

$$(c\underline{\alpha}\cdot\vec{\mathrm{p}}+\beta m_0c^2+V)\Psi_{n\vec{k}}=W_{n\vec{k}}\Psi_{n\vec{k}}, \tag{12}$$

where $\Psi_{n\vec{k}}$ is a four-component function and $\underline{\alpha}$ and β are the 4×4 Dirac matrices.

$$\underline{\alpha}=\begin{pmatrix}0 & \underline{\sigma}\\ \underline{\sigma} & 0\end{pmatrix},\quad \beta=\begin{pmatrix}1 & 0\\ 0 & -1\end{pmatrix}.$$
$$\sigma_x=\begin{pmatrix}0 & 1\\ 1 & 0\end{pmatrix},\quad \sigma_y=\begin{pmatrix}0 & -i\\ i & 0\end{pmatrix},\quad \sigma_z=\begin{pmatrix}1 & 0\\ 0 & -1\end{pmatrix} \tag{13}$$

are the Pauli spin matrices $\underline{\mathrm{p}}=-i\hbar\nabla$, m_0 is the rest mass of electron, $W_{n\vec{k}}$ is the relativistic energy including rest mass, $V(\vec{r})$ is the periodic potential, and n and $\vec{k}$ represent the band index and the reduced wave vector, respectively.

In the RAPW[23] method $\psi_{n\vec{k}}$ is expanded in terms of basis functions $\phi^s_{n\vec{k}}(\vec{K}_i,\vec{r})$:

$$\Psi_{n\vec{k}}=\sum_{i,s}C^s_{n\vec{k}}(\vec{K}_i)\,\phi^s_{n\vec{k}}(\vec{K}_i,\vec{r}) \tag{14}$$

and the $C^s_{n\vec{k}}(\vec{K}_i)$ are determined by solving the variational secular equation.

The crystal potential is decomposed into three different terms:

$$V(\vec{r})=V_{\mathrm{MT}}(\vec{r})+V_{\mathrm{WMT}}(\vec{r})+V_{\mathrm{NS}}(\vec{r}). \tag{15}$$

V_{MT} is the muffin tin which consists of the first term of the expansion for each region: the spherical term within the MT spheres and the constant term in the interstitial region. V_{WMT} is the remaining Fourier expansion in the interstitial region and V_{NS} is the remaining cubic harmonic expansion in the MT spheres. To include the effects of V_{WMT} and V_{NS}, we need only add the matrix elements of these terms to the matrix elements of variational expression and solve the secular equation. This amounts to performing a variation on the general potential with a basis set constructed using the muffin-tin potential. Within the MT spheres, this represents a slight restriction in the variational freedom but as the effects of the nonspherical terms are small, this should be entirely negligible. This need not be true, of course, for very strongly deformed systems but such systems are not our concern here. The RAPW basis functions have the dual representation[23] of the form

$$\phi^s_{n\vec{k}}(\vec{K}_i,\vec{r})=\begin{cases}\begin{pmatrix}\chi(s)\\ \sim 0\end{pmatrix}e^{i\vec{k}_i\cdot\vec{r}}, & r\geq R\\ \sum_{\kappa\mu}A^s_{\kappa\mu}\begin{pmatrix}g_{n\kappa}(r) & \chi_{\kappa\mu}(\hat{r})\\ (i/c)f_{n\kappa}(r) & \chi_{-\kappa\mu}(\hat{r})\end{pmatrix}, & r\leq R\end{cases} \tag{16}$$

which dictated the representation used for the potential. Here $\vec{k}_i=\vec{k}+\vec{K}_i$, where $\vec{K}_i$ is a reciprocal-lattice vector;

$$\chi(\tfrac{1}{2})=\begin{pmatrix}1\\ 0\end{pmatrix};\ \text{and}\ \ \chi(-\tfrac{1}{2})=\begin{pmatrix}0\\ 1\end{pmatrix}$$

are the Pauli spinors; and

$$\chi_\kappa(\hat{r})=\sum_{s=\pm1/2}C(l\tfrac{1}{2}j;\,\mu-s,s)\,Y_l^{\mu-s}(\hat{r})\,\chi(s)$$

are the spin angular functions. C is the Clebsch-Gordan coefficient[22] for $j=\frac{1}{2}$. κ is any nonzero integer such that

$$\kappa=l\ \text{ for } j=l-\tfrac{1}{2},\quad \kappa=-(l+1)\ \text{ for } j=l+\tfrac{1}{2}.$$

The radial functions $g_{n\kappa}$ and $f_{n\kappa}$ satisfy the coupled radial differential equations for a trial energy parameter E_n. (The subscript n is used to denote this energy.) The coefficients $A^s_{\kappa\mu}$ are determined such that the large components are continuous over the boundary of the MT sphere.

The matrix elements of V_{WMT} are merely its Fourier transform since the basis functions are plane waves in this region. Of course, it is necessary to actually perform the Fourier transform[6,7] of the expression of Eq. (1) since that plane-wave expansion does not contain the requirement that V_{WMT} be zero within the muffin-tin spheres except by the limitation of range. The Fourier transform need only be multiplied by a Kroniker δ function on the spin index (s and s'), since the relativistic effects in this term are negligible (order $|V_{\mathrm{WMT}}|/mc^2$ relative to the size of the correction). The inclusion of V_{WMT} is thus quite simple and requires a negligible amount of additional computational effort.

The matrix elements for V_{NS} are rather more complicated:

$$\langle\phi^s(\vec{k}_i;\vec{r})|\,V_{\mathrm{NS}}\,|\phi^{s'}(\vec{k}_j,\vec{r})\rangle$$
$$=(1/\Omega)\sum_{\kappa\kappa'}\frac{i^{(l-l')}j_{l'}(k_iR)j_l(k_jR)}{g_{\kappa'}(R)g_\kappa(R)}\sum_\lambda R_{\kappa\kappa'\lambda}D^{ss'}_{\kappa\kappa'\lambda}, \tag{17a}$$

$$D^{ss'}_{\kappa\kappa'\lambda} = (4\pi)^2 \sum_{\mu} \sum_{\mu'} C(\kappa'\mu's')\, C(\kappa\mu s)\, Y^{\mu}_{l'}{}^{-s}(\hat{k}_i) \times Y^{*\mu'-s'}_{l}(\hat{k}_j) \langle \chi_{\kappa'\mu'} | K_\lambda | \chi_{\kappa\mu} \rangle, \quad (17b)$$

$$R_{\kappa\kappa'\lambda} = \int dr\, r^2\, V_\lambda(r) [g_\kappa g_{\kappa'} + (1/c^2) f_\kappa f_{\kappa'}]. \quad (17c)$$

As noted above, the values of l and j are given by the single index κ. Thus we have given the arguments of the Clebsch-Gordan coefficients in terms of κ, μ and s. In this expression, j_l is a spherical Bessel function and should not be confused with the quantum number j. A straightforward evaluation of this expression proves quite inefficient and expensive so some care must be used to evaluate these matrix elements. The radial ($R_{\kappa\kappa'\lambda}$) and angular ($D^{ss}_{\kappa\kappa'\lambda}$) parts of these matrix elements can each be evaluated in a much simpler fashion.

By studying the $R_{\kappa\kappa'\lambda}$ energy dependence, one finds that it is a quite slowly varying function if one uses orbitals normalized within the MT spheres. A cubic fit was found to reproduce the results in an energy range between 0.0 and 1.2 Ry to better than 0.01%. Thus we determine these polynomial fits at the outset and use them for all the hard calculations.

To evaluate the $D^{ss'}_{\kappa\kappa'\lambda}$, the summation on μ is performed analytically. This yields a result which can be written

$$D^{ss'}_{\kappa\kappa'\lambda}(k_i, k_j) = \langle s | M_\kappa(k_i) I_{ll'\lambda}(k_i, k_j) M^{+}_{\kappa'}(k_j) | s' \rangle, \quad (18a)$$

where

$$M_\kappa(k) = |\kappa| + S_\kappa \vec{\sigma} \cdot \vec{L}(\vec{k}), \quad (18b)$$

$$I_{ll'\lambda}(k_i, k_j) = \int P_l(\hat{k}_i \cdot \hat{r}) K_\lambda P_{l'}(\hat{k}_j \cdot \hat{r}) d^2r, \quad (18c)$$

where S_κ is the sign of κ; P_l is the Legendre polynomial; and the $L(\vec{k})$ is the angular momentum operator for $\vec{k}$. The result will contain a product of Gaunt coefficients and explicit functions of the angles of the wave vectors. Since there are only a few Gaunt coefficients, they can be evaluated and stored once and for all. All terms of Eq. (18) involving a spin-orbit term have been neglected. These remaining terms are actually zero for no spin-orbit coupling through the cancellation of the different j (sign of κ) contributions for the same l. They are thus a correction of order ξ/W to the already small V_{NS} matrix element where ξ is the spin-orbit parameter and W is the bandwidth. Actual numerical tests against the results of the full expression show that, for Nb, a maximal upper bound in the eigenvalue error made by this omission is less that 0.0001 Ry. This is well below the precision sought (of 0.001 Ry). The omission of these terms greatly reduces the complexity of the calculation and thus considerably reduces the effort (cost!).

The κ summations in Eq. (17) were carried through $l(\kappa) \leq 4$ for good convergence of the sums. This limit was determined by examining the convergence for the case where the basis functions were plane waves written as RAPW's. The matrix element calculated could then be compared with the analytic result. Truncation beyond $l = 4$ gave errors compatible with the omission of the spin-orbit components of this term (0.001 Ry). Truncation at $l = 3$ gave errors as large as 50% and at $l = 2$ occasionally gave results of the wrong sign.

Using the above approximations and techniques, it was found that the calculation for eigenvalues and eigenvectors took roughly 25% longer than for the muffin-tin approximation alone. Almost all of this increase was for the nonspherical terms.

III. RESULTS

We now compare three separate band calculations for this overlapping density model: (a) its muffin-tin approximation; (b) the full general (shape) potential, and (c) the inclusion of V_{WMT} but not V_{NS}. This intermediate calculation is included as it has been postulated that V_{WMT} should be the dominant muffin-tin correction[24] and this intermediate approximation requires much less effort. Energies and wave functions were calculated on a regular cubic mesh of linear dimension $(\pi/4a)$ in the $\frac{1}{48}$ th of the Brillouin zone. The resultant energy bands for the general potential (GP) are shown in Fig. 3. It is revealing to note that the size of the non-muffin-tin effects are sufficiently small that it would be difficult, if not impossible,

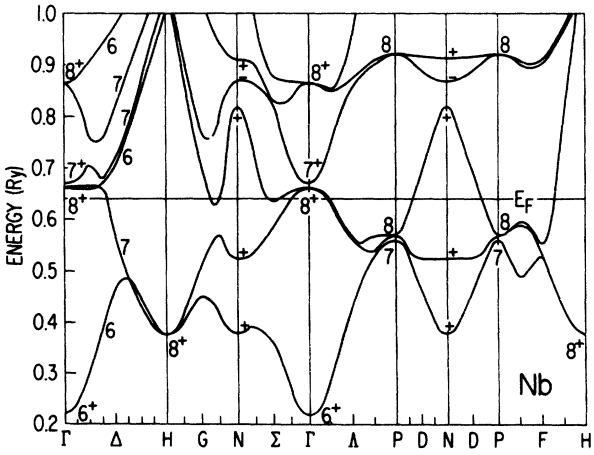

FIG. 3. Energy bands resulting from the overlapping charge-density model with the Slater-exchange approximation when no shape approximations (i.e., MT or WMT) have been made.

TABLE I. Energies (in mRy) found using various shape approximations. The nonrelativistic equivalent representations have been included for convenient comparison to nonrelativistic calculations.

		E_{MT}	E_{WMT}	E_{GP}	δE_{WMT}	δE_{GP}
Γ_1	Γ_{6^+}	220.8	221.5	221.6	0.7	0.8
$\Gamma_{25'}$	Γ_{8^+}	674.7	666.9	661.6	−7.8	−13.1
	Γ_{7^+}	683.5	675.6	670.2	−7.9	−13.3
Γ_{12}	Γ_{8^+}	858.2	860.7	865.9	2.5	7.7
H_{12}	H_{8^+}	370.3	374.9	380.0	4.6	9.7
$H_{25'}$	H_{8^+}	1026.3	1025.1	1023.9	−1.2	−2.4
	H_{7^+}	1038.9	1037.6	1036.3	−1.3	−2.6

to display the differences on a plot of this scale. The comparisons of the three calculations will be separated into three categories: the energies (eigenvalues); the wave functions (eigenvectors); and the Fermi surface. Although the Fermi surface is but another aspect of the energy spectrum, it is one that deserves special attention and accordingly has been given it.

A. Energies

The energy levels at Γ and H are shown in Table I. These two points have been chosen since they have full cubic symmetry and thus their symmetry labels yield a maximum of information. The Γ_6^+ level (s state) is hardly affected by the NMT interactions as it is rather spherically symmetric. The remaining levels in Table I are all d states and, being more anisotropic, are more strongly affected. The t_{2g} (xy like) levels are lowered and the ϵ_g ($3z^2 - r^2$ like) are raised. This is the correction used by Wakoh and Yamashita[12] to adjust their KKR band structures.

To obtain a more global view of the effects on the band structure, we have performed a Fourier-series fit to the RAPW data points. As the bands have Γ_1 symmetry, the expansion coefficients of all vectors of a star (of primitive translations in real space) will be equal. Thus we expand in star functions which are a symmetric combination of all members of a star.[25] For the 55 data points, we least-squares fit 30 star functions yielding fits with an rms error of 4–5 mRy. For the MT and GP calculations, additional points (near the Fermi energy) were calculated such that 53 stars were used to fit 100 data points. This reduced the rms error to 1.8–1.9 mRy. These Fourier-series fits were then used to perform all further eigenspectrum analysis.

The average energy of the band is given by the $\vec{K} = 0$ function ($f = 1$). These values have been tabulated in Table II for all three calculations. This value is actually far more precise then the rms error of the fit. (By comparing the two fits for the MT and GP calculations, we would estimate that the value is precise to 0.1 mRy). Table II also includes the bandwidths which are obtained merely as the energy difference between the highest and lowest energy in the band. As can be seen, the bandwidth is rather more sensitive to the inclusion of non-muffin-tin terms than the band position as noted previously.[6]

TABLE II. Bandwidth and center of the first six bands for the three calculations. The bandwidth is defined as the energy separation of the highest and lowest energy in the band. The center is the average energy (i.e., first moment) of the band. Energies are in mRy.

	Width			Center		
Band	MT	WMT	GP	MT	WMT	GP
1	342.4	339.2	337.1	434.6	434.6	435.0
2	304.4	292.0	281.6	553.2	551.2	550.5
3	462.8	467.5	469.9	660.5	658.6	657.4
4	342.8	349.5	353.7	828.0	825.1	824.8
5 [a]	289.6	285.4	282.4	926.2	922.5	923.1
6 [a]	513.3	495.3	470.8	1006.1	992.2	1007.7

[a] Calculations of center performed with reduced precision as these bands are well above the Fermi energy.

The inclusion of relativistic effects causes more hybridization of bands, the s band lowering relative to d bands, the triply degenerate nonrelativistic level $\Gamma_{25'}$ splitting into "doubly degenerate" Γ_{8^+} and "singly degenerate" Γ_{7^+} with an energy separation of about 9 mRy. (Note that we are factoring out the spin-flip degeneracy in our discussion of the relativistic bands.) The splitting of the doubly degenerate Λ_3 band and the anticrossing of the G_3 and G_4 bands near the Fermi energy, owing to spin-orbit interaction have significant effects on the topology of the Fermi surface. This will complicate comparison with the nonrelativistic results of PFS. Nonetheless, we have compared the shifts owing to the nonspherical potential with those given by PFS with good overall agreement. We especially focused on the shifts in the energy levels at points of high symmetry and along the Σ symmetry line. We found, however, that the WMT terms had a somewhat larger effect than the nonspherical terms, whereas PFS found them to be roughly equal in importance. This can perhaps be understood as a limitation in the variational freedom of the basis functions used by PFS. They used KKR wave functions through $l = 4$ for the interior of the muffin-tin sphere region which were then extended into the interstitial region using the spherical and Neuman Bessel functions. This is a severe truncation of a procedure that would be exact if carried to infinite order. Thus their basis functions are no longer solutions of the muffin-tin potential and

do not have adequate flexibility to fully respond to V_{WMT}.

The density of states was obtained for the MT and GP cases using the tetrahedron decomposition of the irreducible wedge.[26] The MT calculation yielded N_{MT} ($E_F = 0.6455$ Ry) = 10.5 states/Ry/spin while the GP yielded N_{GP} ($E_F = 0.6412$ Ry) = 11.2 states/Ry/spin. The shift in Fermi energy (4.5 mRy) is slightly larger than the shift in the center of band 2 (2.7 mRy) and band 3 (3.1 mRy). As the Fermi energy falls on the upper side of a peak so the density of states is rapidly falling (dn/dE = −350 states/Ry/Ry/spin); this increase in the density of states can be understood as an "almost rigid" band effect.

B. Wave functions

To investigate the NMT effects on the wave functions, we first consider the matrix elements of an approximate angular momentum projection operator using the wave functions obtained for the two

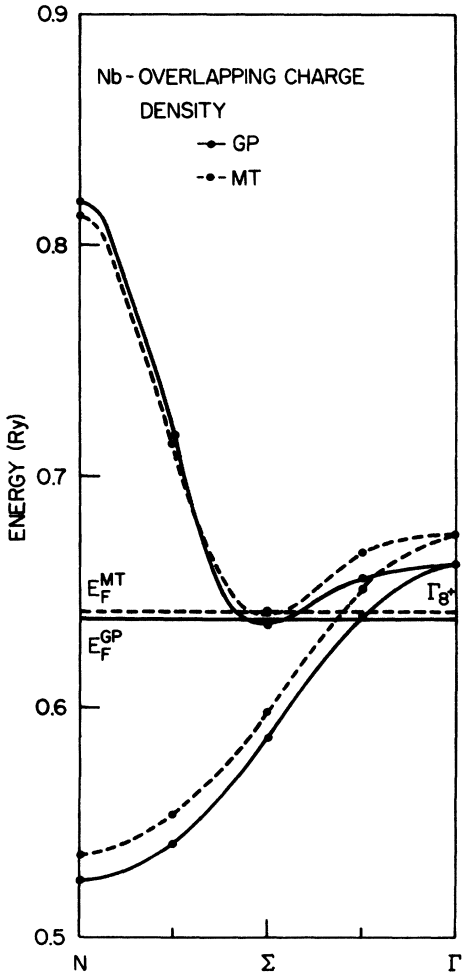

FIG. 4. Comparison of the bands found along Σ with those resulting from the muffin-tin approximation.

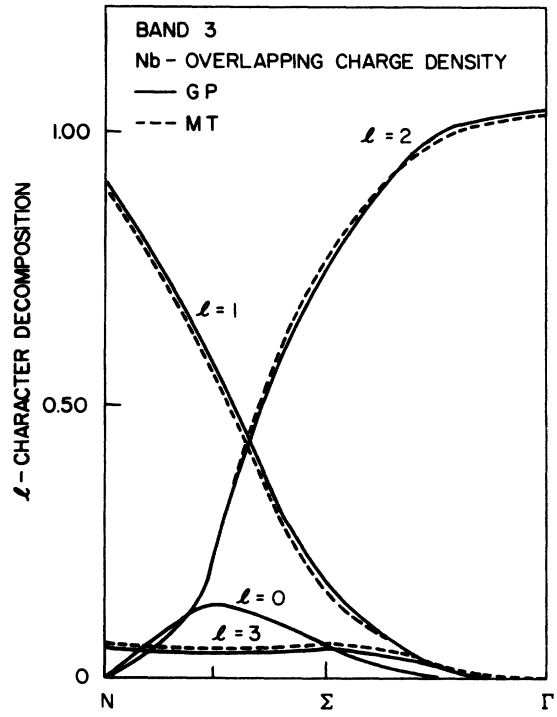

FIG. 5. Angular momentum decomposition along the line Σ. For clarity, we have shown an l decomposition by summing the components for $j = (l + \frac{1}{2})$ and $j = (l - \frac{1}{2})$.

cases of an MT and a general potential. This very crude index involves extending the j character to the Wigner-Seitz radius using spherical Bessel and Neuman functions and thus mainly reflects the changes inside the MT spheres. By expanding the scale, we show the non-muffin-tin energy shifts along the Σ direction in Fig. 4 and the angular momentum decomposition for band 3 in Fig. 5. As can be seen, the s character is relatively unchanged but the NMT terms increase the p character and decrease the f character, while the d and g ($l = 4$) characters first increase and then decrease as one crosses the zone from Γ to N. Band 2 is essentially unchanged by the NMT terms in the Σ direction. This is not surprising as it is pure d-like in this direction. Examining the other symmetry directions, one finds the same trends: p character increases, f character decreases, d character increases near the zone center and decreases near the zone edge. s character is affected only in the region of an anticrossing with a d band and then is generally increased. These effects are never greater than about 5%.

One expects to find larger effects in the interstitial region away from the dominating ionic potential. To examine this, we have calculated the charge densities resulting from each of the calculations. As might be expected, the gross features are not greatly changed. The interstitial charge

of 1.365 electrons for the MT is reduced slightly to 1.353 for the WMT and 1.351 for the GP calculations. Making a spherical harmonic decomposition at the MT radius, we find that the $l=0$ component is increased by 2%. On the other hand, the $l=4$ component is more than doubled and the $l=6$ component more than tripled. The primary effect is to increase the charge in the direction of the near-neighbor atoms. At the unit-cell surface, the charge is increased by 9% in the $\langle 111\rangle$ (nn) direction and decreased by 6% in the $\langle 100\rangle$ and $\langle 110\rangle$ directions.

C. Fermi surface

A model for the Fermi surface of niobium was proposed by Mattheiss[15] and generally confirmed by experimental data[16] and further theoretical calculations.[17] However, none of the previous calculations have taken into account the NMT and relativistic effects. The relativistic terms in the Hamiltonian give rise to the splitting of Γ centered hole octahedron and jungle-gym sheets of Fermi surface. The NMT terms tend to increase the volume of N-centered distorted ellipsoids and decrease the size of the surfaces near Γ.

To obtain the calculated Fermi-surface areas, given in Table III and the cross section shown in Fig. 6, we have used the 53 star-function Fourier fit. The areas were calculated using an orbit tracing routine which obtained the required gradients by finite differences.

The average percent error for the MT calculation is 4.0% over the nine orbits for which both experimental data and MT results exist. This is in good agreement with 4.4% for Mattheiss[15] indicating that relativistic effects are small—at least for these orbits. (We will compare these extensively to Mattheiss with the view that this a good representation of a nonrelativistic MT calculation for the model. We thus assume the small difference in lattice constant used to be negligible.) For these same nine orbits, the GP calculation yielded an average percent error of 10.7%.

The non-muffin-tin terms are seen to have a dramatic *qualitative* effect on the hole octahedron where they produce two additional orbits (α' and β). They sufficiently deform the octahedron that it begins to have features more like the jack in Mo than an octahedron. This quite naturally resolves the speculations[16] about the origins of the α' and β orbits.

We have also tabulated in Table III the band masses. As can be seen, one other effect of the non-muffin-tin terms was to increase the masses by roughly 9% in agreement with the increase in density of states (7%). This was also the average percent difference.

Finally, it is worth noting one other feature of the Fermi surface which has little to do with the non-muffin-tin terms (and probably not with the relativistic effects either). In Fig. 6, one observes a protrusion in the $\Gamma-P-N$ plane on the

TABLE III. Fermi-surface cross sectional areas (in a.u.) and band masses (in electron masses).

Field direction	Orbit [a]	Calculated areas b	Calculated areas MT	Calculated areas GP	Experimental areas c	Experimental areas d	Calculated masses b	Calculated masses MT	Calculated masses GP
[100]	OCT(Γ)	0.247	0.269	0.244	···	···	−1.92	−1.93	−2.23
	OCT(Δ)−β	···	···	0.020	···	0.023	···	···	−0.43
	OCT(Δ)−α'	···	···	0.023	0.035	0.035	···	···	−0.39
	ELL(N)−$\nu_{1,2}$	0.180	0.166	0.194	0.178	0.179	−0.97	−0.91	−1.09
	ELL(N)−ν_{3-6}	0.239	0.223	0.243	0.228	0.228	−0.83	−0.88	−1.06
	JG(Δ)−α	0.033	0.036	0.029	0.039	0.039	−0.57	−0.55	−0.46
	JG(N)	0.418	0.406	0.431	···	···	1.74	1.86	2.11
[111]	OCT(Γ)	0.127	0.136	0.100	···	···	−1.54	−1.47	−1.43
	ELL(N)−$\nu_{1,3,4}$	0.186	0.177	0.194	0.181	0.180	−0.73	−0.74	−0.85
	ELL(N)−$\nu_{2,5,6}$	0.243	0.238	0.256	0.228	0.227	−1.12	−1.09	−1.19
	JG(Γ)	0.208	0.227	0.195	···	···	−2.29	−2.33	−2.69
	JG(H)−η	0.526	0.518	0.500	0.521	0.521	−1.17	−1.04	−1.01
[110]	OCT(Γ)	0.189	0.204	0.172	···	···	−1.66	−1.78	−1.92
	ELL(N)−ν_{3-6}	0.189	0.179	0.199	0.184	0.184	−0.79	−0.75	−0.86
	ELL(N)−ν_1	0.213	0.220	0.234	0.212	0.212	−0.70	−0.70	−0.74
	ELL(N)−ν_2	0.263	0.254	0.270	0.240	0.240	−0.98	−0.91	−0.96

[a] Notation used in Refs. 15–17.
[b] Reference 15.
[c] Halloran *et al.*, Ref. 16.
[d] Scott and Springford, Ref. 16.

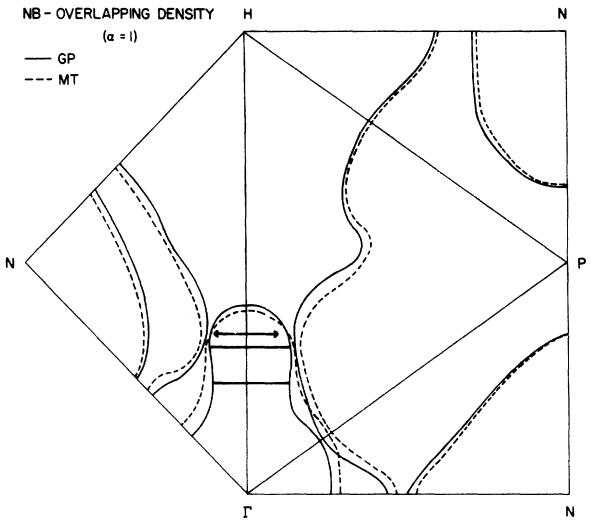

FIG. 6. Fermi-surface cross sections in the symmetry planes. Two bars shown as the "hole octahedron" are the two newly found orbits. Arrows indicate the position of the nearby found jungle-gym orbit.

jungle-gym arm which is, at best, only hinted at in the results of Mattheiss[15] and the reduced lattice-constant results of Anderson *et al.*[17] This protrusion is insufficient to produce extra orbits in the [100] direction. However, it is adequate to explain the anomalies in the η orbits seen by Halloran *et al.*[16] We have plotted calculated orbits for their Fig. 4 and find anomolies at the same angles (within $\pm 3°$). We also find that there is another similar anomoly below 30° with a jump to much larger frequency (0.65 to 0.8 a.u.) and a dramatic increase in mass (*band* mass of 3.5). These may well prove unobservable.

IV. CONCLUSIONS

We have presented here a detailed discussion of a procedure for including the non-muffin-tin terms into the RAPW method. Using the overlapping charge-density model, we have explored the significance of removing the muffin-tin shape approximation and found it to be quite important. The non-muffin-tin terms result in energy shifts consistent with the empirical adjustments made by Wakoh and Yamashita.[12] Most significantly, they are found to produce two de Haas–van Alphen orbits which are not otherwise present in the calculation. Overall, the GP calculation yields somewhat poorer calculated cross-sectional areas which is probably revealing deficiencies in the overlapping charge-density model: surely it is less likely for such a crude model to get structure correctly than to get the average features (MT). We find that the interstitial (WMT) correction is the major non-muffin-tin correction in contrast to PFS.[8] This we attribute to the truncation of their basis functions at $L = 4$ in the interstitial region. The dominant change produced in the wave functions is to direct more charge along the bonding direction.

ACKNOWLEDGMENTS

The authors would like to thank Dr. W. H. Butler, Dr. G. W. Crabtree, Dr. J. B. Ketterson, and Dr. L. R. Windmiller for useful discussions. We are grateful to G. W. Crabtree for bringing our attention to the α' and β orbits and to D. Karim, G. W. Crabtree, J. B. Ketterson, and L. R. Windmiller for access to their unpublished data.

---

*Based on work performed under the auspices of the U. S. Energy Research and Development Administration.

†Paper based in part on a thesis submitted by one of the authors (N. Elyashar) in partial fulfillment of the requirements for the Ph.D. degree at the University of Illinois, Chicago Circle Campus.

‡Present address: Physics Dept., Case Western Reserve University, Cleveland, Ohio 44106.

[1]J. C. Slater, Phys. Rev. 51, 846 (1937); T. L. Loucks, *Augmented Plane Wave* (Benjamin, New York, 1967).

[2]W. Kohn and N. Rostoker, Phys. Rev. 94, 1111 (1954); J. Korringa, Physica (Utr.) 13, 392 (1947).

[3]J. O. Dimmock, Solid State Phys. 26, 103 (1971); L. F. Mattheiss, J. H. Wood, and A. C. Switendick, *Methods of Computational Physics* (Academic, New York, 1968), Vol. 8.

[4]L. F. Mattheiss, A. I. P. Conf. Proc. 4, 57 (1972).

[5]P. D. DeCicco, Phys. Rev. 153, 931 (1967).

[6]D. D. Koelling, A. J. Freeman, and F. M. Mueller, Phys. Rev. B 1, 1318 (1970); H. Schlosser and P. M. Marcus, Phys. Rev. 131, 2529 (1963).

[7]D. D. Koelling, Phys. Rev. 188, 1049 (1969).

[8]G. S. Painter, J. S. Faulkner, and G. M. Stocks, Phys. Rev. B 9, 2448 (1974). (It should be noted that several figures in this paper are actually in Hartree's but are mislabeled as Rydbergs.)

[9]W. E. Rudge, Phys. Rev. 181, 1020 (1969); 181, 1024 (1969).

[10]E. O. Kane, Phys. Rev. B 4, 1917 (1971).

[11]L. Kleinman and R. Shurtleff, Phys. Rev. 188, 1111 (1969); R. Shurtleff and L. Kleinman, Phys. Rev. B 3, 2418 (1971); L. Kleinman and R. Shurtleff, *ibid.* B 4, 3284 (1971).

[12]S. Wakoh and J. Yamashita, J. Phys. Soc. Jpn. 35, 1394 (1973).

[13]J. B. Ketterson, D. D. Koelling, J. C. Shaw, and L. R. Windmiller, Phys. Rev. B 11, 1447 (1975).

[14]D. E. Ellis and G. S. Painter, *Computational Methods in Band Theory*, edited by P. M. Marcus, J. F. Janak,

and A. R. Williams (Plenum, New York, 1971).
[15]L. F. Mattheiss, Phys. Rev. B 1, 373 (1970).
[16]M. H. Holloran, J. H. Condon, J. E. Graebner, J. E. Kunzler, and F. S. L. Hsu, Phys. Rev. B 1, 366 (1970); G. B. Scott and M. Springford, Proc. R. Soc. Lond. A 320, 115 (1970), G. Crabtree, J. B. Ketterson, and L. R. Windmiller (private communication).
[17]J. R. Anderson, D. A. Papaconstantopoulos, J. W. McCaffrey, and J. E. Schirber, Phys. Rev. 87, 5115 (1973).
[18]F. C. Von Der Lage and H. A. Bethe, Phys. Rev. 71, 612 (1947).
[19]N. Elyashar, Ph.D. thesis (University of Illinois, Chicago, 1975) (unpublished).
[20]F. W. De Wette and B. R. A. Nijboer, Physica (Utr.) 24, 1105 (1958).
[21]J. C. Slater, Phys. Rev. 81, 385 (1951).
[22]M. E. Rose, *Relativistic Electron Theory* (Wiley, New York, 1961).
[23]T. L. Loucks, Phys. Rev. 139, A1333 (1965).
[24]J. C. Slater and P. De Cicco, Solid State and Molecular Theory Group, Quarterly Progress Reports, M.I.T., No. 50, p. 46 (1963) (unpublished).
[25]R. Maglic and F. M. Mueller, Int. J. Magnetism 1, 512 (1971).
[26]G. Lehmann and M. Taut, Phys. Status Solidi 54, 469 (1972); G. Lehmann, P. Rennert, M. Taut, and H. Wohn, Phys. Status Solidi 37, K27 (1970); O. Jepsen and O. K. Andersen, Solid State Commun. 9, 1763 (1971); J. Rath and A. J. Freeman, Phys. Rev. 11, 2109 (1975).